

Restoring ergodicity in a strongly disordered interacting chain

B. Krajewski,¹ L. Vidmar,^{2,3} J. Bonča,^{3,2} and M. Mierzejewski¹

¹*Department of Theoretical Physics, Faculty of Fundamental Problems of Technology, Wrocław University of Science and Technology, 50-370 Wrocław, Poland*

²*Department of Theoretical Physics, J. Stefan Institute, SI-1000 Ljubljana, Slovenia*

³*Department of Physics, Faculty of Mathematics and Physics, University of Ljubljana, SI-1000 Ljubljana, Slovenia*

(Dated: January 12, 2023)

We consider a chain of interacting fermions with random disorder that was intensively studied in the context of many-body localization. We show that only a small fraction of the two-body interaction represents a true local perturbation to the Anderson insulator. While this true perturbation is nonzero at any finite disorder strength W , it decreases with increasing W . This establishes a view that the strongly disordered system should be viewed as a weakly perturbed integrable model, i.e., a weakly perturbed Anderson insulator. As a consequence, the latter can hardly be distinguished from a strictly integrable system in finite-size calculations at large W . We then introduce a rescaled model in which the true perturbation is of the same order of magnitude as the other terms of the Hamiltonian, and show that the system remains ergodic at arbitrary large disorder.

Introduction. The interplay between disorder and interactions in quantum systems has recently attracted significant interest. Some of the most exciting ideas were formulated within the framework of many-body localization (MBL), which is conjectured to be as a phase of matter that violates ergodicity in spite of presence of interactions [1–7].

The disordered systems exhibit several unusual properties, in particular extremely slow dynamics [8–15] that was frequently interpreted as a precursor to MBL [16–23]. However, one of the the most important questions about MBL is related to its stability in the thermodynamic limit. Until recently, the results of essentially all studies in one-dimensional (1D) spin-1/2 systems with disorder were interpreted in terms of a stable MBL phase [8–12, 24–48]. Recent work has, however, highlighted robustness of ergodicity at moderate disorder [49], which may eventually suggest that stability of MBL may not be taken for granted. Signatures of robustness of ergodicity were also reported in several subsequent works [14, 15, 50–54] and they triggered, among others, activities to gain a better insight into the avalanche theory of ergodicity breaking transitions [55–62]. However, many recent numerical studies are interpreted in terms of existence of a stable MBL phase [60, 63–80]. Then, the MBL-to-thermal phase transition may occur at much stronger disorders than suggested by earlier numerical calculations [60].

Motivated by these open questions, it is an outstanding problem to understand why exact numerical studies can give rise to formulation of contradictory expectations for the same models in the thermodynamic limit. More generally, what are the crucial ingredients of interacting systems with disorder that make identification of their key physical properties so challenging?

This Letter provides new perspective into studies of robustness of ergodicity and its detection in finite systems. For the model of interacting spinless fermions with disorder, which is mappable onto the paradigmatic random-field Heisenberg chain, we show that only a small fraction

of the two-body interaction represents a true local perturbation to the Anderson insulator. The true perturbation decreases with increasing the disorder, and it eventually becomes too weak to be captured by finite-size numerical calculations. Consequently, the strongly disordered system should be viewed as a weakly perturbed Anderson insulator. As an application of this insight, we introduce a rescaled model in which the strength of the true perturbation matches the energy density of the Anderson insulator. We argue that the latter model remains ergodic at essentially any finite disorder, and show that the matrix elements of observables are consistent with the eigenstate thermalization hypothesis (ETH) [81–84].

Set-up. We study interacting fermions in a 1D disordered lattice with L sites and periodic boundary conditions. The system is described by the Hamiltonian $H = H_0 + H_\Delta$, referred to as the *standard model* further on. The first term describes the Anderson insulator,

$$H_0 = \sum_{i=1}^L h_i, \quad (1)$$

$$h_i = \frac{1}{2}(a_{i+1}^\dagger a_i + \text{H.c.}) + \frac{\epsilon_i}{2}(n_i - \frac{1}{2}) + \frac{\epsilon_{i+1}}{2}(n_{i+1} - \frac{1}{2}),$$

where ϵ_i is a random potential with box distribution, $-W \leq \epsilon_i \leq W$, a_i^\dagger creates a spinless fermion at site i and $n_i = a_i^\dagger a_i$. The second term is the two-body interaction,

$$H_\Delta = \Delta \sum_{i=1}^L N_i, \quad N_i = \left(n_i - \frac{1}{2}\right) \left(n_{i+1} - \frac{1}{2}\right), \quad (2)$$

where we take $\Delta = 1$ so that H can be mapped onto to the widely studied random-field Heisenberg model. The noninteracting part (i.e., the integrable part) of the Hamiltonian is diagonal in the Anderson basis

$$H_0 = \sum_{\alpha} \varepsilon_{\alpha} Q_{\alpha} + \text{const}, \quad Q_{\alpha} = 2a_{\alpha}^{\dagger} a_{\alpha} - 1, \quad (3)$$

where $a_{\alpha} = \sum_i u_{i\alpha}^* a_i$ and $u_{i\alpha} = \langle i | \alpha \rangle$ are components of the single-particle wavefunction of the Anderson state α .

As a central step of our approach, we split the interaction term in Eq. (2) into two orthogonal parts,

$$H_{\Delta} = H_{\Delta}^{\parallel} + H_{\Delta}^{\perp}, \quad \text{with} \quad \langle H_{\Delta}^{\parallel} H_{\Delta}^{\perp} \rangle = 0, \quad (4)$$

where orthogonality is defined via the Hilbert-Schmidt inner product as $\langle AB \rangle = \frac{1}{Z} \text{Tr}(A^{\dagger} B)$, the trace is carried out over many-body states and Z is the dimension of the Fock space. In Eq. (4), H_{Δ}^{\parallel} represents a projection of H_{Δ} onto local integrals of motion of the Anderson insulator, thus $[H_{\Delta}^{\parallel}, H_0] = 0$. As a consequence, we identify the interaction in H_{Δ}^{\perp} as a *true perturbation* to the Anderson insulator, and we argue that it represents a local Hamiltonian. The idea of our approach is sketched in Fig. 1(a). Here, locality of operators (e.g., h_i or N_i) refers to the size of their support in real space which is fixed and does not grow with L . Linear combinations of the latter operators (e.g., H_0 or H_{Δ}) are also considered as local.

Below we show that the squared norm of the true perturbation, $\|H_{\Delta}^{\perp}\|^2$, decays asymptotically for large W as $1/W^2$, whereas the squared norm of the Anderson model, $\|H_0\|^2$, grows as W^2 . Then, for sufficiently large W , the perturbation appears to be too weak to break integrability of a finite system. Here, the squared norms of observables are defined as $\|A\|^2 = \langle AA \rangle$.

Local integrals of motion. The traceless operators Q_{α} from Eq. (3) represent the one-body local integrals of motion of the Anderson insulator. We briefly refer to them as LIOMs. We sort them according to the maxima of the single-particle wave-functions, $u_{i\alpha}$, i.e., we find $i_{\alpha} = \max_i |u_{i\alpha}|$ and sort them such that $i_{\alpha} \leq i_{\alpha'}$ for $\alpha \leq \alpha'$. Roughly speaking, for open boundary conditions the Anderson states with $\alpha \ll L$ are localized at the left edge of the system whereas the states with $\alpha \sim L$ are localized at the right edge. Importantly, a remarkable property of the Anderson insulator is that not only the LIOMs Q_{α} are local, but so are also their products, $Q_{\alpha,d}^{(2)} \equiv Q_{\alpha} Q_{\alpha+d}$, provided that the distance $d = 1, \dots, d_{max}$ is small compared to L and d_{max} does not grow with the system size [85]. We briefly refer to these $Q_{\alpha,d}^{(2)}$ as two-body LIOMs.

It is straightforward to show that H_{Δ} from Eq. (2) has no projection on traceless LIOMs Q_{α} , see [86] for details. Therefore, we introduce an operator N_i^{\parallel} that is a linear combination of two-body LIOMs, such that

$$N_i^{\parallel} = \sum_{d=1}^{d_{max}} \sum_{\alpha=1}^L \langle Q_{\alpha,d}^{(2)} N_i \rangle Q_{\alpha,d}^{(2)}, \quad N_i^{\perp} = N_i - N_i^{\parallel}. \quad (5)$$

The operator N_i^{\parallel} can be interpreted as a projection of a local interaction onto two-body LIOMs, and hence it corresponds to an interaction that does not break integrability of the Anderson insulator. In contrast, N_i^{\perp} can be viewed as the true perturbation.

We stress two important technical details. First, we only consider results for $d_{max} = 2$ in this Letter, whereas in [86] we show that additional contributions coming from

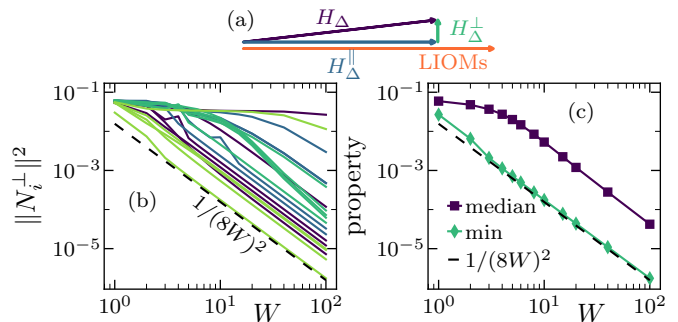


Figure 1. (a) Sketch of the construction in Eq. (4). (b) Dependence of $\|N_i^{\perp}\|^2$ on W , where various curves correspond to different i but the same disorder realization [we keep $\epsilon_i/W = \text{const}$ when increasing W]. Various colors correspond to different realizations of disorder. (c) Two statistical properties of $\|N_i^{\perp}\|^2$ from 10^4 curves as those in (b): median and minimum. Dashed line is the lower bound $1/(8W)^2$, see [86]. Results in (b,c) are obtained at $L = 14$ and $L/2$ fermions.

$d_{max} > 2$ are negligible at strong disorder. Second, in the Fock space that consists of 2^L many-body configurations, the occupations of LIOMs Q_{α} are independent and their products $Q_{\alpha,d}^{(2)}$ are mutually orthogonal and normalized, i.e., $\langle Q_{\alpha,d}^{(2)} Q_{\alpha',d'}^{(2)} \rangle = \delta_{\alpha,\alpha'} \delta_{d,d'}$. As a consequence, Eq. (5) represents an orthogonal projection for which $\langle N_i^{\parallel} N_i^{\perp} \rangle = 0$. However, the actual calculations are carried out in a subspace with $L/2$ fermions, in which the LIOMs are not independent since $\sum_{\alpha} Q_{\alpha} = 0$, and their products are not traceless since $\langle Q_{\alpha,d}^{(2)} \rangle = O(1/L)$. Then, one needs to reorthogonalize the set of $Q_{\alpha,d}^{(2)}$, as explained in [86].

Norm of the true perturbation. We can now express H_{Δ}^{\parallel} and H_{Δ}^{\perp} from Eq. (4) using Eq. (5) as

$$H_{\Delta}^{\parallel} = \Delta \sum_{i=1}^L N_i^{\parallel} \quad \text{and} \quad H_{\Delta}^{\perp} = \Delta \sum_{i=1}^L N_i^{\perp}. \quad (6)$$

Since Eq. (5) assures locality of N_i^{\parallel} and N_i^{\perp} , then H_{Δ}^{\parallel} and H_{Δ}^{\perp} are also local as they are defined as linear combinations of local operators N_i and $Q_{\alpha,d}^{(2)}$. The physical meaning of H_{Δ}^{\perp} can be understood by inspecting the identity (see [86] for a derivation)

$$\|H_{\Delta}^{\perp}\|^2 = \|H_{\Delta}\|^2 - \sum_{\alpha,d} \langle H_{\Delta} Q_{\alpha,d}^{(2)} \rangle^2, \quad (7)$$

which shows that the more two-body LIOMs $Q_{\alpha,d}^{(2)}$ one takes, the smaller is the norm of H_{Δ}^{\perp} . Indeed, the essence of our approach is a systematic elimination of local contributions to H_{Δ} which commute with the integrable Hamiltonian H_0 .

Figures 1(b) and 1(c) study the dependence on W of the squared norms $\|N_i^{\perp}\|^2$ that contribute to the norm of H_{Δ}^{\perp} in Eq. (6). Each curve in Fig. 1(b) is obtained

for a single site i and a single realization of disorder, while Fig. 1(c) shows the median and the minimum of 10^4 curves as those in Fig. 1(b). One observes huge fluctuations between various sites and disorder realizations. Nevertheless, at sufficiently large W all curves eventually decay as $\|N_i^\perp\|^2 \propto 1/W^2$, see Fig. 1(b). For strong disorder we establish an L -independent bound $\|N_i^\perp\|^2 \geq 1/(8W)^2$, which accurately reproduces the numerical results in Fig. 1(c) already at $W > 3$. The derivation of the bound and the L -dependence of $\|N_i^\perp\|^2$ are discussed in [86].

Summarizing this part, we stress that the perturbation to the Anderson insulator is not determined by the entire interaction term but rather by the projected operators, N_i^\perp . This perturbation becomes very weak at strong disorder, $\|N_i^\perp\| \sim 1/W$, but remains nonzero for arbitrary finite W . Obviously, such a small but non-vanishing perturbation poses a challenge for finite-size numerical calculations.

Ergodicity in the rescaled model. We complement the above analysis by introducing a model in which the norm of the true perturbation does not vanish with increasing W . To this end we study the *rescaled model* Hamiltonian

$$\tilde{H} = \sum_i h_i + \sum_i \frac{\|h_i\|}{\|N_i^\perp\|} N_i^\perp, \quad (8)$$

where h_i denotes the local term (the energy density operator) of the Anderson model from Eq. (1) and N_i^\perp represents the density of the true perturbation from Eq. (6). Both energy density operators h_i and N_i are defined on the link between sites i and $i+1$.

The rescaled model (8) associates the strength of the perturbation with the strength of the disorder. In particular, the energy density of the true perturbation, cf. the second term on the r.h.s. of Eq. (8), equals to the energy density of the Anderson insulator, for which the squared norm is $\|h_i\|^2 = (2 + \epsilon_i^2 + \epsilon_{i+1}^2)/16$. In the standard model, this roughly corresponds to the regime $\Delta \propto W$, for which one may expect an ergodic-to-nonergodic transition. (The nonergodic phase is conjectured to be reentrant as a function of the interaction strength, see, e.g., Fig. 1 in [12].) Below we explore robustness of ergodicity in the rescaled model (8).

As a simple test of ergodicity we study the average ratio of nearest level spacings $\langle r \rangle$ (i.e., the gap ratio), see [86] for a definition. The results are shown in Figs. 2(a) for the standard model H from Eqs. (1)-(2) and in Fig. 2(b) for the rescaled model \tilde{H} from Eq. (8). In the standard model the results clearly deviate from the value $r \simeq 0.53$ in the Gaussian orthogonal ensemble (GOE) already at $W \gtrsim 3$, which was observed in many previous studies, see, e.g., Refs. [29]. However, the rescaled model remains ergodic at essentially all disorders, provided that the system is sufficiently large. As an additional test, we determine a distribution of r without any averaging, i.e., via collecting results from different disorder realizations as well as different eigenstates (from the middle third

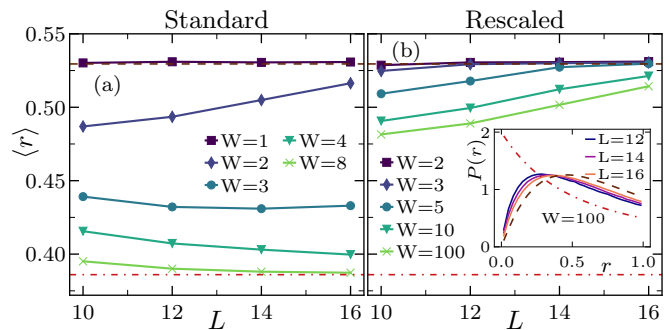


Figure 2. Average gap ratio, $\langle r \rangle$, at various L and W calculated in subspaces with $L/2$ fermions for (a) the standard model H from Eqs. (1)-(2) and (b) the rescaled model \tilde{H} from Eq. (8). The averaging is carried out over $Z/3$ levels from the middle of the spectrum and over 4000 realizations of disorder. Inset in (b): probability density function $P(r)$ in the rescaled model at $W = 100$ and various L . Dash-dotted and dashed lines show the analytical predictions for the Poisson distribution [3] and the GOE [87, 88], respectively (see also [86]).

of spectra). The inset of Fig. 2(b) shows the resulting probability density function $P(r)$ at various L . A comparison with analytical results [3, 86–89] confirms that at large L the results approach the GOE prediction even at $W = 100$.

ETH analysis. Finally, we test ergodicity of the rescaled Hamiltonian by studying the ETH. As observables we consider site occupations $A_i = 2n_i - 1$. Note that a linear combination of A_i , the imbalance $I = \sum_i (-1)^i A_i$, has been commonly studied in the context of ergodic-nonergodic transition and is accessible in cold-atom experiments [90]. Following a standard procedure [83], we calculate the diagonal matrix elements $(A_i)_m = \langle E_m | A_i | E_m \rangle$ where $|E_m\rangle$ are the many-body eigenstates of either the standard Hamiltonian H , or the rescaled Hamiltonian \tilde{H} , see Fig. 3. In a finite system described by the standard model, one observes $(A_i)_m = \pm 1$ at all energies at strong disorder, see Figs. 3(c) and 3(e), and hence the ETH appears to be violated, suggesting nonergodic behavior. However, in the rescaled model the fluctuations of matrix elements are rather modest even at extremely strong disorder $W = 100$, see Fig. 3(f).

To study fluctuations of the diagonal matrix elements we calculate the average eigenstate-to-eigenstate fluctuations [91–93],

$$\langle \delta A \rangle = 1/Z \sum_m |(A_i)_{m+1} - (A_i)_m|, \quad (9)$$

where the averaging is carried out over $Z = Z/5$ states from the middle of the many-body spectrum. Figure 4 shows the probability density functions, $f(\langle \delta A \rangle)$, calculated at a single lattice site and different disorder realizations, for both the standard and the rescaled model. In the standard model one obtains $\langle \delta A \rangle \simeq 1$ at large disorder [cf. Figs. 4(c) and 4(e)], and the absence of any visible L -dependence of the distributions may be inter-

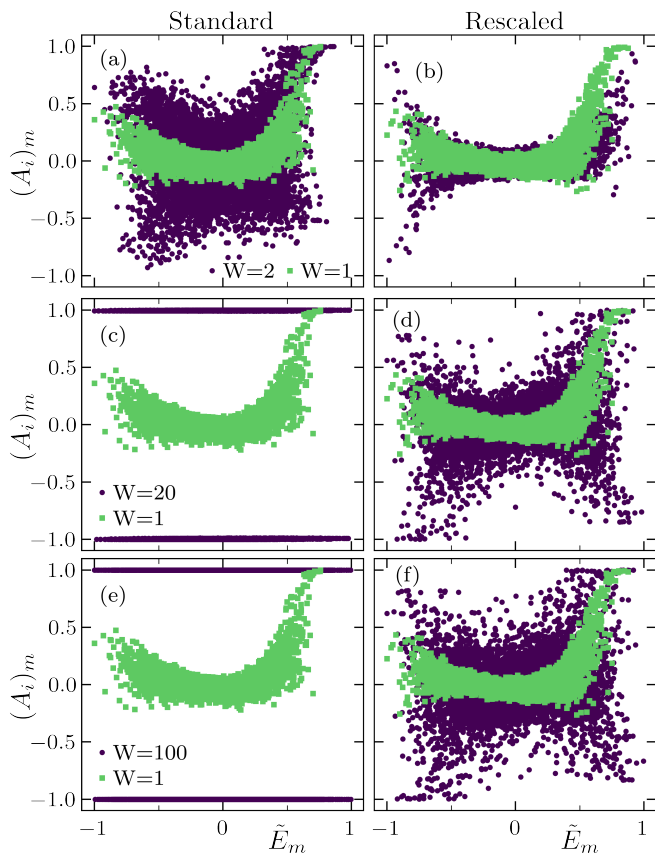


Figure 3. Diagonal matrix elements $(A_i)_m = \langle E_m | A_i | E_m \rangle$, where $A_i = 2n_i - 1$, at $L = 16$ and different W . Results are shown for a single site i and a single realization of disorder. (a,c,e) The standard model H from Eqs. (1)-(2) and (b,d,f) the rescaled model \tilde{H} from Eq. (8). We rescale the energies as $\tilde{E}_m = E_m/|E_0|$, where E_0 is the ground state energy.

interpreted as a violation of the ETH. In the rescaled model the distribution of $\langle \delta A \rangle$ is rather broad for the accessible system sizes. Nevertheless $\langle \delta A \rangle$ appears to decay with L suggesting $\langle \delta A \rangle \rightarrow 0$ in the thermodynamic limit. Due to the width of the distributions, one cannot unambiguously confirm exponential decay of the latter quantity. However, such a decay is strongly suggested by the decay of the median, see also [86].

Conclusions. The main goal of this Letter was to identify the origin of complexity that emerges in the numerical studies of ergodicity in interacting fermions subject to random disorder. We showed that the two-body interaction term H_Δ (2) cannot be considered as a perturbation to the Anderson insulator H_0 (1) since only a small fraction of the two-body interaction, denoted as H_Δ^\perp , does not commute with H_0 . We referred to the latter as the true local perturbation and we showed that its relative norm decays with disorder as $\|H_\Delta^\perp\|/\|H_0\| \sim W^{-2}$. On the other hand, the norm is also bounded from below so it remains nonzero at large but finite W . It is then clear that the interpretation of finite-size numerical calculations at large W is challenging since finite integrable

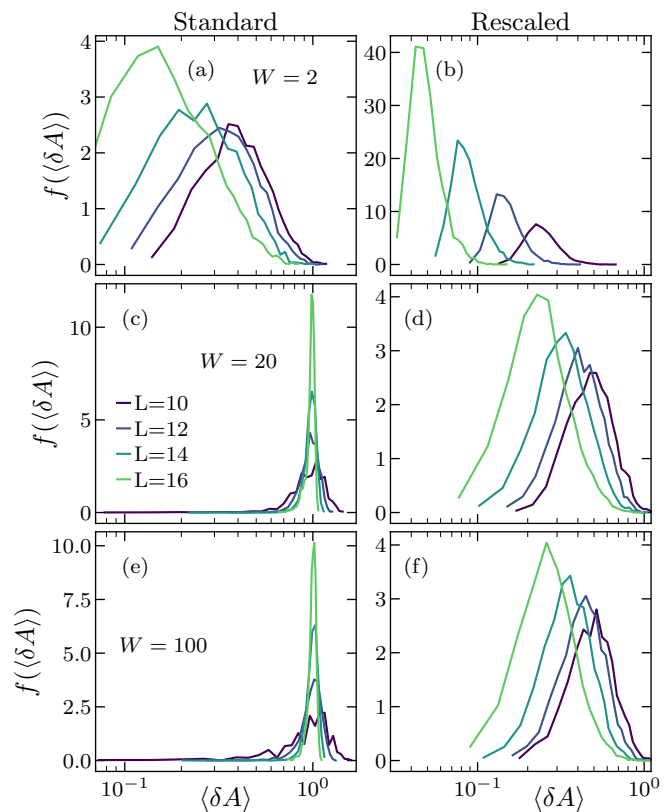


Figure 4. Probability density function f of the eigenstate-to-eigenstate fluctuations $\langle \delta A \rangle$ from Eq. (9) for various L . The distributions are calculated at single lattice site and different realizations of disorder for (a,c,e) the standard model H and (b,d,f) the rescaled model \tilde{H} .

systems with small perturbations are hardly distinguishable from strictly integrable systems.

It appears that the two regimes in which interpretation of numerical results has rather low ambiguity are: the regime of small and moderate W , for which robustness of ergodicity was already established, and the regime where the strength of the true local perturbation H_Δ^\perp is rescaled. Here we considered the latter scenario and introduced a rescaled model in which the energy density of the perturbation equals that of the Anderson insulator. Studying the short-range level statistics and the ETH indicators in the rescaled model we showed that ergodicity persists up to extremely strong disorders, such as $W = 100$.

While focusing on 1D interacting fermions with random disorder, the main idea of our approach can be applied to an arbitrary model in any dimension. In particular, the method of identifying the true local perturbation allows for an unambiguous classification of the perturbation strength, and hence provides a new perspective into distinction between weakly and strongly perturbed integrable systems. Systems of broad interest to which the method can straightforwardly be applied in the near future are interacting fermions subject to quasiperiodic [94]

or linear [95, 96] potentials.

ACKNOWLEDGMENTS

We acknowledge discussions with M. Rigol. We acknowledge the support by the National Science Cen-

tre, Poland via project 2020/37/B/ST3/00020 (B.K and M.M.), the support by the Slovenian Research Agency (ARRS), Research Core Fundings Grants P1-0044 (L.V. and J.B.) and J1-1696 (L.V.).

-
- [1] D. Basko, I. Aleiner, and B. Altshuler, Metal–insulator transition in a weakly interacting many-electron system with localized single-particle states, *Ann. Phys.* **321**, 1126 (2006).
- [2] I. V. Gornyi, A. D. Mirlin, and D. G. Polyakov, Interacting electrons in disordered wires: Anderson localization and low- t transport, *Phys. Rev. Lett.* **95**, 206603 (2005).
- [3] V. Oganesyan and D. A. Huse, Localization of interacting fermions at high temperature, *Phys. Rev. B* **75**, 155111 (2007).
- [4] R. Nandkishore and D. A. Huse, Many-body-localization and thermalization in quantum statistical mechanics, *Ann. Rev. Cond. Mat. Phys.* **6**, 15 (2015).
- [5] E. Altman and R. Vosk, Universal dynamics and renormalization in many-body-localized systems, *Annu. Rev. Condens. Matter Phys.* **6**, 383 (2015).
- [6] F. Alet and N. Laflorencie, Many-body localization: An introduction and selected topics, *C. R. Physique* **19**, 498 (2018).
- [7] D. A. Abanin, E. Altman, I. Bloch, and M. Serbyn, Colloquium: Many-body localization, thermalization, and entanglement, *Rev. Mod. Phys.* **91**, 021001 (2019).
- [8] M. Žnidarič, T. Prosen, and P. Prelovšek, Many-body localization in the Heisenberg XXZ magnet in a random field, *Phys. Rev. B* **77**, 064426 (2008).
- [9] M. Serbyn, Z. Papić, and D. A. Abanin, Universal slow growth of entanglement in interacting strongly disordered systems, *Phys. Rev. Lett.* **110**, 260601 (2013).
- [10] J. A. Kjäll, J. H. Bardarson, and F. Pollmann, Many-body localization in a disordered quantum Ising chain, *Phys. Rev. Lett.* **113**, 107204 (2014).
- [11] S. Bera, H. Schomerus, F. Heidrich-Meisner, and J. H. Bardarson, Many-body localization characterized from a one-particle perspective, *Phys. Rev. Lett.* **115**, 046603 (2015).
- [12] Y. Bar Lev, G. Cohen, and D. R. Reichman, Absence of diffusion in an interacting system of spinless fermions on a one-dimensional disordered lattice, *Phys. Rev. Lett.* **114**, 100601 (2015).
- [13] M. Serbyn, Z. Papić, and D. A. Abanin, Thouless energy and multifractality across the many-body localization transition, *Phys. Rev. B* **96**, 104201 (2017).
- [14] D. Sels and A. Polkovnikov, Dynamical obstruction to localization in a disordered spin chain, *Phys. Rev. E* **104**, 054105 (2021).
- [15] L. Vidmar, B. Krajewski, J. Bonča, and M. Mierzejewski, Phenomenology of spectral functions in disordered spin chains at infinite temperature, *Phys. Rev. Lett.* **127**, 230603 (2021).
- [16] D. J. Luitz and Y. Bar Lev, Anomalous thermalization in ergodic systems, *Phys. Rev. Lett.* **117**, 170404 (2016).
- [17] D. J. Luitz and Y. Bar Lev, The ergodic side of the many-body localization transition, *Ann. Phys. (Berl.)* **529**, 1600350 (2016).
- [18] M. Žnidarič, A. Scardicchio, and V. K. Varma, Diffusive and subdiffusive spin transport in the ergodic phase of a many-body localizable system, *Phys. Rev. Lett.* **117**, 040601 (2016).
- [19] S. Gopalakrishnan, K. R. Islam, and M. Knap, Noise-induced subdiffusion in strongly localized quantum systems, *Phys. Rev. Lett.* **119**, 046601 (2017).
- [20] M. Kozarzewski, P. Prelovšek, and M. Mierzejewski, Spin subdiffusion in the disordered Hubbard chain, *Phys. Rev. Lett.* **120**, 246602 (2018).
- [21] P. Prelovšek and J. Herbrych, Self-consistent approach to many-body localization and subdiffusion, *Phys. Rev. B* **96**, 035130 (2017).
- [22] Y. B. Lev, D. M. Kennes, C. Klöckner, D. R. Reichman, and C. Karrasch, Transport in quasiperiodic interacting systems: From superdiffusion to subdiffusion, *EPL (Europhysics Letters)* **119**, 37003 (2017).
- [23] P. Prelovšek, J. Bonča, and M. Mierzejewski, Transient and persistent particle subdiffusion in a disordered chain coupled to bosons, *Phys. Rev. B* **98**, 125119 (2018).
- [24] A. Pal and D. A. Huse, Many-body localization phase transition, *Phys. Rev. B* **82**, 174411 (2010).
- [25] C. Monthus and T. Garel, Many-body localization transition in a lattice model of interacting fermions: Statistics of renormalized hoppings in configuration space, *Phys. Rev. B* **81**, 134202 (2010).
- [26] E. Khatami, M. Rigol, A. Relaño, and A. M. García-García, Quantum quenches in disordered systems: Approach to thermal equilibrium without a typical relaxation time, *Phys. Rev. E* **85**, 050102 (2012).
- [27] J. H. Bardarson, F. Pollmann, and J. E. Moore, Unbounded growth of entanglement in models of many-body localization, *Phys. Rev. Lett.* **109**, 017202 (2012).
- [28] A. De Luca and A. Scardicchio, Ergodicity breaking in a model showing many-body localization, *EPL (Europhysics Letters)* **101**, 37003 (2013).
- [29] D. J. Luitz, N. Laflorencie, and F. Alet, Many-body localization edge in the random-field Heisenberg chain, *Phys. Rev. B* **91**, 081103 (2015).
- [30] E. J. Torres-Herrera and L. F. Santos, Dynamics at the many-body localization transition, *Phys. Rev. B* **92**, 014208 (2015).
- [31] M. Serbyn, Z. Papić, and D. A. Abanin, Criterion for many-body localization-delocalization phase transition, *Phys. Rev. X* **5**, 041047 (2015).
- [32] T. Devakul and R. R. P. Singh, Early breakdown of area-law entanglement at the many-body delocalization transition, *Phys. Rev. Lett.* **115**, 187201 (2015).

- [33] M. Serbyn and J. E. Moore, Spectral statistics across the many-body localization transition, *Phys. Rev. B* **93**, 041424 (2016).
- [34] C. L. Bertrand and A. M. García-García, Anomalous Thouless energy and critical statistics on the metallic side of the many-body localization transition, *Phys. Rev. B* **94**, 144201 (2016).
- [35] M. Mierzejewski, J. Herbrych, and P. Prelovšek, Universal dynamics of density correlations at the transition to the many-body localized state, *Phys. Rev. B* **94**, 224207 (2016).
- [36] R. Steinigeweg, J. Herbrych, F. Pollmann, and W. Brenig, Typicality approach to the optical conductivity in thermal and many-body localized phases, *Phys. Rev. B* **94**, 180401 (2016).
- [37] M. Filippone, P. W. Brouwer, J. Eisert, and F. von Oppen, Drude weight fluctuations in many-body localized systems, *Phys. Rev. B* **94**, 201112 (2016).
- [38] V. Khemani, S. P. Lim, D. N. Sheng, and D. A. Huse, Critical properties of the many-body localization transition, *Phys. Rev. X* **7**, 021013 (2017).
- [39] V. Khemani, D. N. Sheng, and D. A. Huse, Two universality classes for the many-body localization transition, *Phys. Rev. Lett.* **119**, 075702 (2017).
- [40] G. De Tomasi, S. Bera, J. H. Bardarson, and F. Pollmann, Quantum mutual information as a probe for many-body localization, *Phys. Rev. Lett.* **118**, 016804 (2017).
- [41] F. Pietracaprina, G. Parisi, A. Mariano, S. Pascazio, and A. Scardicchio, Entanglement critical length at the many-body localization transition, *J. Stat. Mech.* (2017), 113102.
- [42] J. Gray, S. Bose, and A. Bayat, Many-body localization transition: Schmidt gap, entanglement length, and scaling, *Phys. Rev. B* **97**, 201105 (2018).
- [43] P. Sierant and J. Zakrzewski, Level statistics across the many-body localization transition, *Phys. Rev. B* **99**, 104205 (2019).
- [44] M. Schiulaz, E. J. Torres-Herrera, and L. F. Santos, Thouless and relaxation time scales in many-body quantum systems, *Phys. Rev. B* **99**, 174313 (2019).
- [45] N. Macé, F. Alet, and N. Laflorencie, Multifractal scalings across the many-body localization transition, *Phys. Rev. Lett.* **123**, 180601 (2019).
- [46] S. Roy, J. T. Chalker, and D. E. Logan, Percolation in Fock space as a proxy for many-body localization, *Phys. Rev. B* **99**, 104206 (2019).
- [47] S. Roy and D. E. Logan, Fock-space correlations and the origins of many-body localization, *Phys. Rev. B* **101**, 134202 (2020).
- [48] M. Tarzia, Many-body localization transition in Hilbert space, *Phys. Rev. B* **102**, 014208 (2020).
- [49] J. Šuntajs, J. Bonča, T. Prosen, and L. Vidmar, Ergodicity breaking transition in finite disordered spin chains, *Phys. Rev. B* **102**, 064207 (2020).
- [50] J. Šuntajs, J. Bonča, T. Prosen, and L. Vidmar, Quantum chaos challenges many-body localization, *Phys. Rev. E* **102**, 062144 (2020).
- [51] M. Kiefer-Emmanouilidis, R. Unanyan, M. Fleischhauer, and J. Sirker, Evidence for unbounded growth of the number entropy in many-body localized phases, *Phys. Rev. Lett.* **124**, 243601 (2020).
- [52] M. Kiefer-Emmanouilidis, R. Unanyan, M. Fleischhauer, and J. Sirker, Slow delocalization of particles in many-body localized phases, *Phys. Rev. B* **103**, 024203 (2021).
- [53] T. LeBlond, D. Sels, A. Polkovnikov, and M. Rigol, Universality in the onset of quantum chaos in many-body systems, *Phys. Rev. B* **104**, L201117 (2021).
- [54] D. Sels and A. Polkovnikov, Thermalization of dilute impurities in one dimensional spin chains, [arXiv:2105.09348](https://arxiv.org/abs/2105.09348) (2021).
- [55] W. De Roeck and F. Huveneers, Stability and instability towards delocalization in many-body localization systems, *Phys. Rev. B* **95**, 155129 (2017).
- [56] D. J. Luitz, F. Huveneers, and W. De Roeck, How a small quantum bath can thermalize long localized chains, *Phys. Rev. Lett.* **119**, 150602 (2017).
- [57] T. Thiery, F. Huveneers, M. Müller, and W. De Roeck, Many-body delocalization as a quantum avalanche, *Phys. Rev. Lett.* **121**, 140601 (2018).
- [58] P. J. D. Crowley and A. Chandran, Avalanche induced coexisting localized and thermal regions in disordered chains, *Phys. Rev. Research* **2**, 033262 (2020).
- [59] D. Sels, Bath-induced delocalization in interacting disordered spin chains, *Phys. Rev. B* **106** (2022).
- [60] A. Morningstar, L. Colmenarez, V. Khemani, D. J. Luitz, and D. A. Huse, Avalanches and many-body resonances in many-body localized systems, *Phys. Rev. B* **105**, 174205 (2022).
- [61] J. Šuntajs and L. Vidmar, Ergodicity Breaking Transition in Zero Dimensions, *Phys. Rev. Lett.* **129**, 060602 (2022).
- [62] P. J. D. Crowley and A. Chandran, Mean field theory of failed thermalizing avalanches, [arXiv:2204.09688](https://arxiv.org/abs/2204.09688).
- [63] R. K. Panda, A. Scardicchio, M. Schulz, S. R. Taylor, and M. Žnidarič, Can we study the many-body localization transition?, *EPL (Europhysics Letters)* **128**, 67003 (2020).
- [64] P. Sierant, D. Delande, and J. Zakrzewski, Thouless time analysis of anderson and many-body localization transitions, *Phys. Rev. Lett.* **124**, 186601 (2020).
- [65] P. Sierant, M. Lewenstein, and J. Zakrzewski, Polynomially filtered exact diagonalization approach to many-body localization, *Phys. Rev. Lett.* **125**, 156601 (2020).
- [66] D. Abanin, J. Bardarson, G. De Tomasi, S. Gopalakrishnan, V. Khemani, S. Parameswaran, F. Pollmann, A. Potter, M. Serbyn, and R. Vasseur, Distinguishing localization from chaos: Challenges in finite-size systems, *Ann. Phys.* **427**, 168415 (2021).
- [67] Á. L. Corps, R. A. Molina, and A. Relaño, Signatures of a critical point in the many-body localization transition, *SciPost Phys.* **10**, 107 (2021).
- [68] A. Prakash, J. H. Pixley, and M. Kulkarni, Universal spectral form factor for many-body localization, *Phys. Rev. Research* **3**, L012019 (2021).
- [69] J. Schliemann, J. V. I. Costa, P. Wenk, and J. C. Egues, Many-body localization: Transitions in spin models, *Phys. Rev. B* **103**, 174203 (2021).
- [70] M. Hopjan, G. Orso, and F. Heidrich-Meisner, Detecting delocalization-localization transitions from full density distributions, *Phys. Rev. B* **104**, 235112 (2021).
- [71] A. Solórzano, L. F. Santos, and E. J. Torres-Herrera, Multifractality and self-averaging at the many-body localization transition, *Phys. Rev. Research* **3**, L032030 (2021).
- [72] G. De Tomasi, I. M. Khaymovich, F. Pollmann, and S. Warzel, Rare thermal bubbles at the many-body lo-

- calization transition from the Fock space point of view, *Phys. Rev. B* **104**, 024202 (2021).
- [73] P. J. D. Crowley and A. Chandran, A constructive theory of the numerically accessible many-body localized to thermal crossover, *SciPost Phys.* **12**, 201 (2022).
- [74] R. Ghosh and M. Žnidarič, Resonance-induced growth of number entropy in strongly disordered systems, *Phys. Rev. B* **105**, 144203 (2022).
- [75] N. Bölter and S. Kehrein, Scrambling and many-body localization in the XXZ chain, *Phys. Rev. B* **105**, 104202 (2022).
- [76] Y. Zhang and Y. Liang, Optimizing randomized potentials for inhibiting thermalization in one-dimensional systems, *Phys. Rev. Research* **4**, 023091 (2022).
- [77] P. Sierant and J. Zakrzewski, Challenges to observation of many-body localization, *Phys. Rev. B* **105**, 224203 (2022).
- [78] J. Sutradhar, S. Ghosh, S. Roy, D. E. Logan, S. Mukerjee, and S. Banerjee, Scaling of the Fock-space propagator and multifractality across the many-body localization transition, *Phys. Rev. B* **106**, 054203 (2022).
- [79] F. B. Trigueros and C.-J. Lin, Krylov complexity of many-body localization: Operator localization in Krylov basis, *SciPost Phys.* **13**, 037 (2022).
- [80] D. Z. Shi, V. Khemani, R. Vasseur, and S. Gopalakrishnan, Many body localization transition with correlated disorder, [arXiv:2204.06017](https://arxiv.org/abs/2204.06017).
- [81] J. M. Deutsch, Quantum statistical mechanics in a closed system, *Phys. Rev. A* **43**, 2046 (1991).
- [82] M. Srednicki, Chaos and quantum thermalization, *Phys. Rev. E* **50**, 888 (1994).
- [83] M. Rigol, V. Dunjko, and M. Olshanii, Thermalization and its mechanism for generic isolated quantum systems, *Nature (London)* **452**, 854 (2008).
- [84] L. D'Alessio, Y. Kafri, A. Polkovnikov, and M. Rigol, From quantum chaos and eigenstate thermalization to statistical mechanics and thermodynamics, *Adv. Phys.* **65**, 239 (2016).
- [85] In contrast, in translationally invariant integrable models the products of local charges are typically nonlocal thus, in the thermodynamic limit, they have no projection on local observables.
- [86] See Supplemental Material for reorthogonalization of LIOMs in the subspace with fixed number of fermions, absence of projection of H_Δ on LIOMs, derivation of Eq. (7) and the lower bound on the norm of the true perturbation, the details about the nearest level spacing analysis and the fluctuations of the diagonal matrix elements.
- [87] Y. Y. Atas, E. Bogomolny, O. Giraud, and G. Roux, Distribution of the ratio of consecutive level spacings in random matrix ensembles, *Phys. Rev. Lett.* **110**, 084101 (2013).
- [88] M. Fremling, Exact gap-ratio results for mixed Wigner surmises of up to 4 eigenvalues, [arXiv:2202.01090](https://arxiv.org/abs/2202.01090) (2022).
- [89] O. Giraud, N. Macé, E. Vernier, and F. Alet, Probing symmetries of quantum many-body systems through gap ratio statistics, *Phys. Rev. X* **12**, 011006 (2022).
- [90] M. Schreiber, S. S. Hodgman, P. Bordia, H. P. Lüschen, M. H. Fischer, R. Vosk, E. Altman, U. Schneider, and I. Bloch, Observation of many-body localization of interacting fermions in a quasi-random optical lattice, *Science* **349**, 842 (2015).
- [91] H. Kim, T. N. Ikeda, and D. A. Huse, Testing whether all eigenstates obey the eigenstate thermalization hypothesis, *Phys. Rev. E* **90**, 052105 (2014).
- [92] R. Mondaini, K. R. Fratus, M. Srednicki, and M. Rigol, Eigenstate thermalization in the two-dimensional transverse field Ising model, *Phys. Rev. E* **93**, 032104 (2016).
- [93] D. Jansen, J. Stolpp, L. Vidmar, and F. Heidrich-Meisner, Eigenstate thermalization and quantum chaos in the Holstein polaron model, *Phys. Rev. B* **99**, 155130 (2019).
- [94] S. Iyer, V. Oganesyan, G. Refael, and D. A. Huse, Many-body localization in a quasiperiodic system, *Phys. Rev. B* **87**, 134202 (2013).
- [95] M. Schulz, C. A. Hooley, R. Moessner, and F. Pollmann, Stark many-body localization, *Phys. Rev. Lett.* **122**, 040606 (2019).
- [96] E. van Nieuwenburg, Y. Baum, and G. Refael, From Bloch oscillations to many-body localization in clean interacting systems, *Proc. Natl. Acad. Sci.* **116**, 9269 (2019).

Supplemental Material: Restoring ergodicity in a strongly disordered interacting chain

B. Krajewski¹, L. Vidmar^{2,3}, J. Bonča^{3,2}, and M. Mierzejewski¹

¹*Department of Theoretical Physics, Faculty of Fundamental Problems of Technology,
Wrocław University of Science and Technology, 50-370 Wrocław, Poland*

²*Department of Theoretical Physics, J. Stefan Institute, SI-1000 Ljubljana, Slovenia*

³*Department of Physics, Faculty of Mathematics and Physics, University of Ljubljana, SI-1000 Ljubljana, Slovenia*

In the Supplemental Material we provide technical details about calculations in the subspace with a fixed number of fermions, absence of projection of H_Δ on LIOMs, the derivation of Eq. (7) and the lower bound on the norm of the true perturbation, the details about the nearest level spacing analysis and the fluctuations of the diagonal matrix elements.

S1. LIOMS IN THE SUBSPACE WITH FIXED NUMBER OF FERMIONS

The derivation of the true perturbation H_Δ^\perp , cf. Eqs. (4)-(6) in the main text, has been carried out in the Fock space of 2^L many-body configurations, i.e., with a variable number of fermions. In this case, the occupations of LIOMs Q_α from Eq. (3) in the main text are independent and their products $Q_{\alpha,d}^{(2)}$ are mutually orthogonal and normalized, i.e.,

$$\langle Q_{\alpha,d}^{(2)} Q_{\alpha',d'}^{(2)} \rangle = \delta_{\alpha,\alpha'} \delta_{d,d'}. \quad (\text{S1})$$

However, the actual numerical calculations presented in the main text have been carried out in a subspace with a fixed number of fermions, $N = L/2$. Then, the LIOMs are not independent because $\sum_{\alpha=1}^L Q_\alpha = 0$. This implies that the exact LIOMs in this subspace are linear combinations of Q_α . Nevertheless, since the interaction H_Δ has no projection on LIOMs, see Sec. S2, we focus below on two-body LIOMs $Q_{\alpha,d}^{(2)}$, which are the central object in introducing the true perturbation in Eqs. (5) and (6). In the subspace of a fixed number of fermions, the two-body LIOMs are neither traceless nor orthonormal. In order to apply the orthogonal projections, see Eq. (5) in the main text, one first needs to construct traceless products, $Q_{\alpha,d}^{(2)} = Q_\alpha Q_{\alpha+d} - \text{const}$, where the constant is set by the condition $\langle Q_{\alpha,d}^{(2)} \rangle = 0$. Then one needs to reorthogonalize the set $\{Q_{\alpha,d}^{(2)}\}$. To this end we solve the eigenproblem

$$\sum_{\alpha'=1}^L \sum_{d'=1}^{d_{\max}} \langle Q_{\alpha,d}^{(2)} Q_{\alpha',d'}^{(2)} \rangle V_{(\alpha',d'),\gamma} = \lambda_\gamma V_{(\alpha,d),\gamma} \quad (\text{S2})$$

for the real symmetric matrix built out of all scalar products of $Q_{\alpha,d}^{(2)}$, i.e., we solve the eigenproblem for $\langle Q_{\alpha,d}^{(2)} Q_{\alpha',d'}^{(2)} \rangle$. Here, $V_{(\alpha,d),\gamma}$ is an orthogonal matrix and

the eigenvalues are positive, $\lambda_\gamma > 0$, for $d_{\max} < L/2 - 1$. We introduce a new set of two-body LIOMs

$$q_\gamma^{(2)} = \sum_{\alpha=1}^L \sum_{d=1}^{d_{\max}} \frac{1}{\sqrt{\lambda_\gamma}} V_{(\alpha,d),\gamma} Q_{\alpha,d}^{(2)}, \quad (\text{S3})$$

which are normalized and mutually orthogonal

$$\begin{aligned} \langle q_\gamma^{(2)} q_{\gamma'}^{(2)} \rangle &= \sum_{\alpha,\alpha'=1}^L \sum_{d,d'=1}^{d_{\max}} \frac{V_{(\alpha,d),\gamma} \langle Q_{\alpha,d}^{(2)} Q_{\alpha',d'}^{(2)} \rangle V_{(\alpha',d'),\gamma'}}{\sqrt{\lambda_\gamma} \sqrt{\lambda_{\gamma'}}} \\ &= \delta_{\gamma,\gamma'} \frac{\lambda_{\gamma'}}{\sqrt{\lambda_\gamma} \sqrt{\lambda_{\gamma'}}} = \delta_{\gamma,\gamma'}. \end{aligned} \quad (\text{S4})$$

The new set of orthonormal two-body LIOMs, $\{q_\gamma^{(2)}\}$, should be used instead of $\{Q_{\alpha,d}^{(2)}\}$ whenever the Fock space is reduced to a subspace with a fixed particle number. We note that the linear transformation in Eq. (S3) of local $Q_{\alpha,d}^{(2)}$ leads to local $q_\gamma^{(2)}$. Therefore the reorthogonalization does not spoil locality of two-body LIOMs.

S2. ABSENCE OF PROJECTION OF H_Δ ON LIOMS

We here show that $H_\Delta = \Delta \sum_i N_i$ from Eq. (2) in the main text has no projection on the LIOMs Q_α , i.e.,

$$\langle N_i Q_\alpha \rangle = 0 \quad \longrightarrow \quad \langle H_\Delta Q_\alpha \rangle = 0. \quad (\text{S5})$$

This statement is valid irrespectively of whether the Hilbert-Schmidt inner product $\langle \dots \rangle$ in Eq. (S5) is calculated in the Fock space (FS) of 2^L basis states, or within a subspace (S) with a fixed particle number $N = L/2$ and dimension $\binom{L}{N}$. To show that we express all operators in the real-space basis and calculate the projection

$$\langle N_i Q_\alpha \rangle = \frac{1}{4} \sum_{j,l} u_{i\alpha}^* u_{j\alpha} \langle (2n_i - 1)(2n_{i+1} - 1)(2a_j^\dagger a_l - \delta_{jl}) \rangle, \quad (\text{S6})$$

where $u_{j\alpha} = \langle j|\alpha\rangle$ are components of the single-particle wavefunction of the Anderson state $|\alpha\rangle$. The only nonzero contributions to Eq. (S6) come from terms corresponding to $l = j$. We note also that $(2n_i - 1)^2 = 1$ and that the operator $2n_i - 1$ is traceless both in FS and S, i.e., $\langle 2n_i - 1 \rangle = 0$. Therefore, the contributions corresponding to $j = i$ or $j = i + 1$ vanish. In particular, for $j = i + 1$ one obtains

$$\langle (2n_i - 1)(2n_{i+1} - 1)^2 \rangle = \langle (2n_i - 1) \rangle = 0. \quad (\text{S7})$$

The remaining contributions should be considered separately for calculations in FS and S. From now on we assume that $j \neq i$ and $j \neq i + 1$ so that all lattice indexes in Eq. (S6) correspond to different lattice sites. The vanishing of $\langle N_i Q_\alpha \rangle$ in FS follows from the independence of occupations of different sites,

$$\begin{aligned} & \langle (2n_i - 1)(2n_{i+1} - 1)(2n_j - 1) \rangle \\ &= \langle (2n_i - 1) \rangle \langle (2n_{i+1} - 1) \rangle \langle (2n_j - 1) \rangle = 0. \end{aligned} \quad (\text{S8})$$

In the subspace S, we note that $\frac{1}{L} \sum_i 2n_i$ is the identity operator, hence we use the identity

$$\begin{aligned} 0 &= \sum_i (2n_i - 1) \sum_j (2n_j - 1) \sum_l (2n_l - 1) \\ &= \sum_{i=j=l} (2n_i - 1)^2 (2n_i - 1) \end{aligned} \quad (\text{S9})$$

$$+ 3 \sum_{i=l \neq j} (2n_i - 1)^2 (2n_j - 1) \quad (\text{S10})$$

$$+ \sum_{i \neq j \neq l, i \neq l} (2n_i - 1)(2n_j - 1)(2n_l - 1). \quad (\text{S11})$$

The contributions in Eqs. (S9) and (S10) represent traceless operators, as it follows from Eq. (S7). Since $\langle (2n_i - 1)(2n_j - 1)(2n_l - 1) \rangle$ does not depend on the lattice indexes (provided that i, j, l are different) one finds that $\langle (2n_i - 1)(2n_j - 1)(2n_l - 1) \rangle = 0$. Therefore, all contributions to the projection $\langle N_i Q_\alpha \rangle$ vanish. It holds true also within the subspace S despite $\langle N_i \rangle$ is not traceless but rather $\langle N_i \rangle = O(1/L)$.

S3. DERIVATION OF EQ. (7)

The r.h.s. of Eq. (7) in the main text corresponds to the norm of the difference

$$\|H_\Delta - H_\Delta^\parallel\|^2 = \langle (H_\Delta - H_\Delta^\parallel)(H_\Delta - H_\Delta^\parallel) \rangle. \quad (\text{S12})$$

Equation (4) implies that $\langle H_\Delta H_\Delta^\parallel \rangle = \langle H_\Delta^2 \rangle$, hence one can rewrite Eq. (S12) as

$$\|H_\Delta - H_\Delta^\parallel\|^2 = \langle H_\Delta^2 \rangle - \langle H_\Delta H_\Delta^\parallel \rangle. \quad (\text{S13})$$

Since $H_\Delta^\parallel = \Delta \sum_i N_i^\parallel$ and using the expression in Eq. (5) for N_i^\parallel , one obtains

$$\langle H_\Delta H_\Delta^\parallel \rangle = \Delta \sum_i \sum_{d,\alpha} \langle Q_{\alpha,d}^{(2)} N_i \rangle \langle H_\Delta Q_{\alpha,d}^{(2)} \rangle = \sum_{d,\alpha} \langle H_\Delta Q_{\alpha,d}^{(2)} \rangle^2. \quad (\text{S14})$$

Plugging Eq. (S14) into Eq. (S13), one obtains the expression on the r.h.s. of Eq. (7) in the main text.

S4. BOUNDS FOR PROJECTED OPERATORS

Here, we study in more details the properties of the projected operators, N_i^\perp , and establish a lower bound on their norm. To this end we use the many-body Anderson states $|\vec{\alpha}\rangle = |\alpha_1, \alpha_2, \dots, \alpha_L\rangle$ and introduce an auxiliary operator

$$\tilde{N}_i = N_i - \sum_{\vec{\alpha}} \langle \vec{\alpha} | N_i | \vec{\alpha} \rangle |\vec{\alpha}\rangle \langle \vec{\alpha}|, \quad (\text{S15})$$

where all diagonal matrix elements have been eliminated. We note that the projection in Eq. (5) in the main text eliminates the diagonal matrix elements of N_i^\perp only partially, hence it is intuitively clear that $\|N_i^\perp\| \geq \|\tilde{N}_i\|$. Below we present a formal proof of this lower bound on $\|N_i^\perp\|$.

We rewrite Eq. (5) in the main text as

$$N_i = N_i^\perp + \sum_{\beta,d} \langle Q_{\beta,d}^{(2)} N_i \rangle Q_{\beta,d}^{(2)} \quad (\text{S16})$$

and note that $Q_{\beta,d}^{(2)}$ are diagonal in the many-body Anderson basis, hence

$$\sum_{\vec{\alpha}} \langle \vec{\alpha} | Q_{\beta,d}^{(2)} | \vec{\alpha} \rangle |\vec{\alpha}\rangle \langle \vec{\alpha}| = Q_{\beta,d}^{(2)}. \quad (\text{S17})$$

Putting Eqs. (S16) and (S17) into the right-hand side of Eq. (S15) one obtains the identity

$$N_i^\perp = \tilde{N}_i + \sum_{\vec{\alpha}} \langle \vec{\alpha} | N_i^\perp | \vec{\alpha} \rangle |\vec{\alpha}\rangle \langle \vec{\alpha}|. \quad (\text{S18})$$

In the Anderson basis, \tilde{N}_i has only off-diagonal matrix elements whereas the second term, $\sum_{\vec{\alpha}} \langle \vec{\alpha} | N_i^\perp | \vec{\alpha} \rangle |\vec{\alpha}\rangle \langle \vec{\alpha}|$, is diagonal. Moreover, the squared Hilbert-Schmidt norm can be explicitly written as a sum of squares of all matrix elements, $\|\dots\|^2 = \frac{1}{Z} \sum_{\vec{\alpha}, \vec{\alpha}'} |\langle \vec{\alpha} | \dots | \vec{\alpha}' \rangle|^2$. The latter two properties combined with Eq. (S18) imply that

$$\|N_i^\perp\|^2 = \|\tilde{N}_i\|^2 + \left\| \sum_{\vec{\alpha}} \langle \vec{\alpha} | N_i^\perp | \vec{\alpha} \rangle |\vec{\alpha}\rangle \langle \vec{\alpha}| \right\|^2 \geq \|\tilde{N}_i\|^2. \quad (\text{S19})$$

Consequently, one obtains the lower bound

$$\|N_i^\perp\|^2 \geq \|\tilde{N}_i\|^2, \quad (\text{S20})$$

which holds true for arbitrary distance d_{max} in Eq. (5) in the main text.

Figure S1 shows correlations between norms of N_i^\perp and \tilde{N}_i for various d_{max} . Each point in this plot shows result for a single site i and a single realization of disorder. These results not only confirm the bound $\|N_i^\perp\| \geq \|\tilde{N}_i\|$

from Eq. (S20) but also demonstrate that for strong disorder (i.e., for small $\|N_i^\perp\|$) the projected operator can be well approximated as $N_i^\perp \simeq \tilde{N}_i$. Comparing Figs. S1(a)-S1(d) one observes that the larger is the distance d_{max} , the better is the approximation. At strong disorder, however, the approximation $N_i^\perp \simeq \tilde{N}_i$ is accurate already for $d_{max} = 2$. It means that the conserved part of the interaction, N_i , is dominated by the projections of N_i on two-body LIOMs $Q_{\alpha,d}^{(2)}$, i.e., by the products of LIOMs corresponding to the neighboring orbitals with $d = 1$ or $d = 2$.

Next, we discuss the origin of the bound $\|N_i^\perp\| \geq 1/(8W)^2$ which was observed from the numerical results shown in the main text in Fig. 1. To this end we show that $\|\tilde{N}_i\| \geq 1/(8W)^2$ and then make use of the inequality (S20). For simplicity we assume that the single-particle wave functions, $u_{i\alpha}$, are real, we express the operator N_i in the Anderson basis

$$\begin{aligned} N_i &= \left(a_i^\dagger a_i - \frac{1}{2} \right) \left(a_{i+1}^\dagger a_{i+1} - \frac{1}{2} \right) \\ &= \sum_{\alpha,\beta,\gamma,\eta} u_{i\alpha} u_{i\beta} \left(a_\alpha^\dagger a_\beta - \frac{\delta_{\alpha,\beta}}{2} \right) u_{i+1\gamma} u_{i+1\eta} \left(a_\gamma^\dagger a_\eta - \frac{\delta_{\gamma,\eta}}{2} \right), \end{aligned} \quad (\text{S21})$$

and recall that \tilde{N}_i represents the off-diagonal contribution to Eq. (S21). The more localized are the Anderson wave-functions the smaller are the off-diagonal contributions to Eq. (S21). Then, it is useful to study a two-site problem for the Anderson Hamiltonian [see Eq. (1) in the main text] with extreme values of the disorder potentials

$$\epsilon_{1,2} = \pm W$$

$$\begin{pmatrix} W & \frac{1}{2} \\ \frac{1}{2} & -W \end{pmatrix} \begin{pmatrix} u_{1\alpha} \\ u_{2\alpha} \end{pmatrix} = \epsilon_\alpha \begin{pmatrix} u_{1\alpha} \\ u_{2\alpha} \end{pmatrix}. \quad (\text{S22})$$

Direct calculations show that $\lim_{W \rightarrow \infty} u_{11} = \lim_{W \rightarrow \infty} u_{22} = 1$, whereas,

$$\lim_{W \rightarrow \infty} W u_{i\alpha} = \pm \frac{1}{4}, \quad i \neq \alpha. \quad (\text{S23})$$

We assume that the lower bound on $\|\tilde{N}_i\|^2$ denoted as $\|N_i^{\text{bound}}\|^2$, can be obtained via introducing single-particle wave-functions from Eq. (S22) into Eq. (S21). In other words, N_i^{bound} corresponds to the most localized orbitals, $u_{i\alpha}$, on two sites. Namely, we assume that for each site i there is a single Anderson state denoted as $\alpha(i)$ such that $u_{i\alpha(i)}$ is of the order $O(1)$, and one other state, $\alpha'(i) \neq \alpha(i)$, for which $u_{i\alpha'(i)} = \pm \frac{1}{4W}$,

$$u_{i\beta} \simeq \delta_{\beta,\alpha(i)} \pm \frac{1}{4W} \delta_{\beta,\alpha'(i)}. \quad (\text{S24})$$

Then, one finds the leading (with respect to $1/W$) contributions to the off-diagonal part of N_i^{bound} ,

$$\begin{aligned} N_i^{\text{bound}} &\simeq \pm \frac{1}{4W} [a_{\alpha'(i)}^\dagger a_{\alpha(i)} + \text{H.c.}] [n_{\alpha(i+1)} - \frac{1}{2}] \\ &\pm \frac{1}{4W} [n_{\alpha(i)} - \frac{1}{2}] [a_{\alpha'(i+1)}^\dagger a_{\alpha(i+1)} + \text{H.c.}]. \end{aligned} \quad (\text{S25})$$

Using the identity $[n_{\alpha(i)} - \frac{1}{2}]|\vec{\alpha}\rangle = \pm \frac{1}{2}|\vec{\alpha}\rangle$ one may simplify Eq. (S25) to

$$\begin{aligned} N_i^{\text{bound}} &\simeq \pm \frac{1}{8W} [a_{\alpha'(i)}^\dagger a_{\alpha(i)} + \text{H.c.}] \\ &\pm \frac{1}{8W} [a_{\alpha'(i+1)}^\dagger a_{\alpha(i+1)} + \text{H.c.}]. \end{aligned} \quad (\text{S26})$$

The resulting N_i^{bound} is a sum of two hopping terms and the squared Hilbert-Schmidt norm of each term equals $\frac{1}{2} \frac{1}{(8W)^2}$. Finally, we find the inequalities

$$\|N_i^\perp\|^2 \geq \|\tilde{N}_i\|^2 \geq \|N_i^{\text{bound}}\|^2 = 1/(8W)^2. \quad (\text{S27})$$

Fig. 1 in the main text demonstrates that $1/(8W)^2$ very accurately reproduces the minimum of $\|N_i^\perp\|^2$ obtained from numerical simulations already for $W > 3$. It follows from Eq. (S24) that the latter bound is applicable only at $1/4W \ll 1$ and it must break down at $W < 0.5$ since $\|N_i^\perp\|^2 \leq \|N_i\|^2 = 1/16$.

Finally we demonstrate that the norms $\|N_i^\perp\|$, shown in Fig. 1 in the main text, weakly depend on the size of the studied system. To this end, we have determined the distributions of the latter quantities for lattices with $L = 12$ and $L = 16$ sites. Figures S2(a) and S2(b) show the probability density functions of $\|N_i^\perp\|$ at $W = 2$ and $W = 20$, respectively. The distributions have been obtained via collecting results for 4000 realizations of disorder and for all sites, $i = 1, \dots, L$. We do not observe any significant L -dependence of these distributions for either weak (left panel) or strong (right panel) disorder.

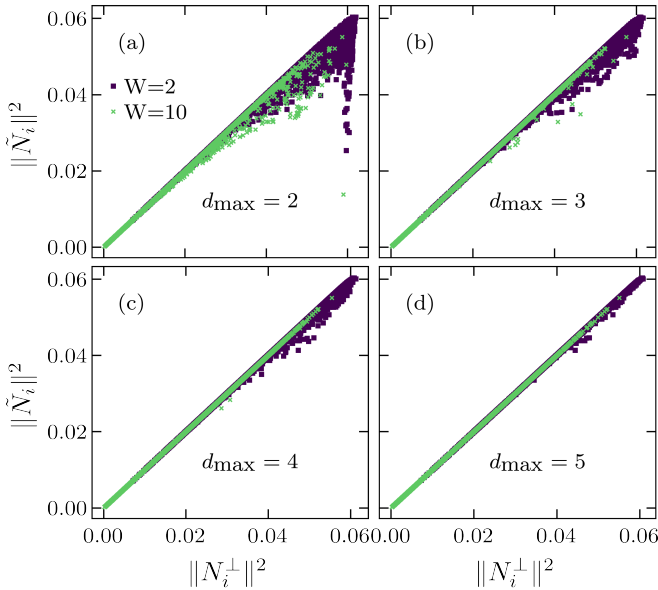


Figure S1. Results for chain with $L = 14$ sites and $L/2$ fermions. Points show $\|N_i^\perp\|$ and $\|\tilde{N}_i\|$ for various sites i , disorder realizations and W . In (a), (b), (c) and (d) we use, respectively, the maximal distance $d_{max} = 2, 3, 4$ and 5 , see Eq. (5) in the main text.

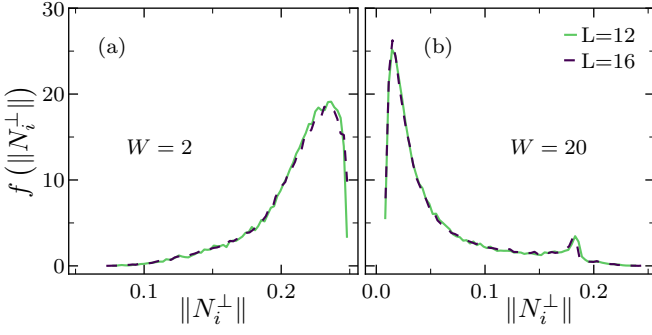


Figure S2. Probability density functions f of $\|N_i^\perp\|$. Results are obtained for 4000 realizations of disorder at $L = 12, 16$ with (a) $W = 2$ and (b) $W = 20$.

S5. NEAREST LEVEL SPACINGS

In Fig. 2 in the main text we studied the statistical properties of the ratio of nearest level spacings, shortly the gap ratio [3]. For a target many-body eigenstate $|E_m\rangle$, the gap ratio is defined as

$$r_m = \frac{\min\{\delta E_m, \delta E_{m-1}\}}{\max\{\delta E_m, \delta E_{m-1}\}}, \quad (\text{S28})$$

where $\delta E_m = E_{m+1} - E_m$ is the level spacing. We then averaged r_m over the middle third of the energy spectrum as well as over 4000 various realizations of disordered. The average gap ratio $\langle r \rangle$ is plotted in the main panels of Figs. 2(a) and 2(b).

In the inset of Fig. 2(b) we plotted a probability density function $P(r)$ that includes results for r_m from Eq. (S28) obtained at different disorder realizations, as well as different target eigenstates $|E_m\rangle$ at a fixed disorder realization. The latter are again obtained from the middle third of the energy spectra. Results are compared to the analytical predictions for the Poisson distribution [3],

$$P(r) = \frac{2}{(1+r)^2}, \quad (\text{S29})$$

see the dash-dotted line the inset of Fig. 2(b), and for the GOE [87],

$$P(r) = \frac{27}{4} \frac{r+r^2}{(1+r+r^2)^{5/2}}, \quad (\text{S30})$$

see the dashed line in the inset of Fig. 2(b).

S6. MATRIX ELEMENTS OF OBSERVABLES

In the main text we studied eigenstate-to-eigenstate fluctuations of the diagonal matrix elements, $\langle \delta A \rangle$, for

a single site occupation, $A = 2n_i - 1$. In particular, we have determined the probability density functions, $f(\langle \delta A \rangle)$ shown in Fig. 4 in the main text. In order to

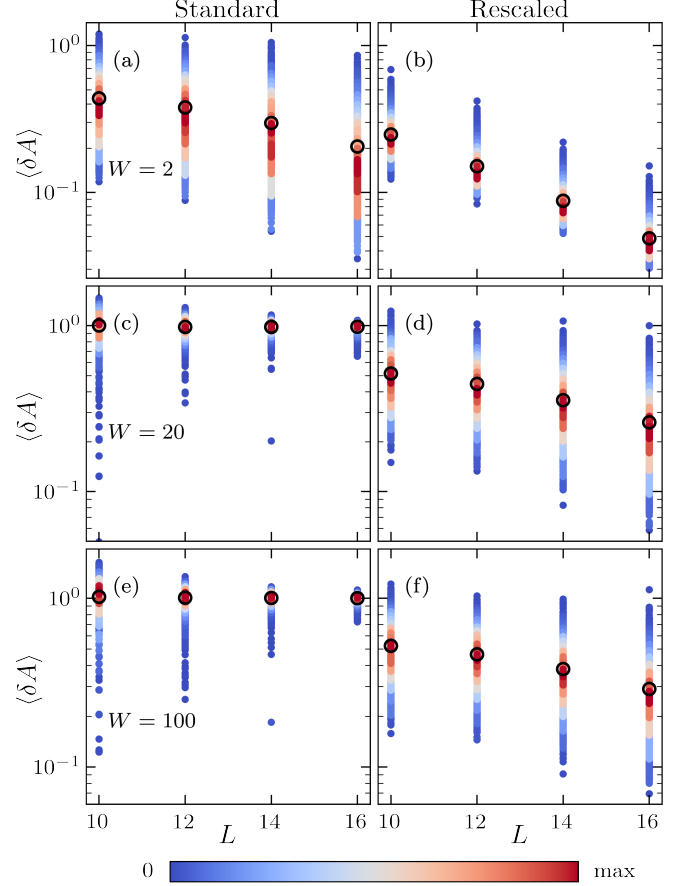


Figure S3. Eigenstate-to-eigenstate fluctuations $\langle \delta A \rangle$ from Eq. (9) in the main text. We first calculate $\langle \delta A \rangle$ for a single lattice occupation, $A = 2n_i - 1$, and different realizations of disorder. Then present a density plot of these values. Open circles show the medians. Panels (a,c,e) show results for the standard model, H , and (b,d,f) for the rescaled model \hat{H} .

better visualize the L -dependence of the eigenstate-to-eigenstate fluctuations, we show in Figure S3 the density plot of $\langle \delta A \rangle$ as a function of the system size. Each point shows result for a single site, i , and a single realization of disorder whereas color marks the density of such points. In the standard model at strong disorder, see Figs. S3(c) and S3(e), one observes strong fluctuations and $\langle \delta A \rangle \sim 1$ for all accessible system sizes. In the rescaled model, see Figs. S3(d) and S3(f), the fluctuations visibly decrease with L , however the probability density function, $f(\langle \delta A \rangle)$, remains broad. Therefore, the L -dependence of the fluctuations can be followed via inspecting the medians (circles) and maxima (red color) of $f(\langle \delta A \rangle)$. Both quantities suggest that fluctuations decay exponentially with L as it is expected for systems which obey the eigenstate thermalization hypothesis.